Eur. Phys. J. A **21**, 407–417 (2004)
DOI 10.1140/epja/i2003-10219-7

THE EUROPEAN PHYSICAL JOURNAL A

The Binary Cascade

Nucleon nuclear reactions

G. Folger, V.N. Ivanchenko, and J.P. Wellisch[a]

CERN, 1211 Geneva 23, Switzerland

Received: 19 December 2003 / Revised version: 5 March 2004 /
Published online: 7 September 2004 –
Communicated by A. Molinari

Abstract. The Binary Cascade introduces a novel approach towards intra-nuclear cascade calculations. Like many QMD codes, it uses a detailed 3-dimensional model of the nucleus, and is based exclusively on binary scattering between reaction participants and nucleons within this nuclear model. Like a classical cascade, it uses optical potentials to describe the time evolution of particles passing through the nuclear medium. In the present paper we introduce the model, and investigate its predictive power for hadron spectra in nucleon nuclear reactions final states.

PACS. 21.60.Ka Nuclear structure: Monte Carlo models – 24.10.Lx Nuclear reactions: general: Monte Carlo simulations (including hadron and parton cascades and string breaking models)

1 Introduction

Many intra-nuclear cascade [1] models have been proposed and developed in the past by several groups. In many cases the motivation was to provide a satisfactory level of description of final-state hadron spectra in the problem of few MeV to few GeV reactions of hadrons with nuclei.

Just like Binary Cascade, they find application in low-energy calorimetry, studies of nucleon shielding, accelerator-based nuclear-waste degradation, neutrino beams, or studies of design and application of spallation neutron sources.

The Binary Cascade introduces a new approach to cascade calculations. It is based on a detailed 3-dimensional model of the nucleus, and exclusively based on binary scattering between reaction participants and nucleons within this nuclear model. This feature makes it a hybrid between a classical cascade code, and a quantum molecular dynamics model (QMD) [2].

In Binary Cascade, like in QMD, each participating nucleon is seen as a Gaussian wave package,

$$\phi(x, q_i, p_i, t) = \\ 2/(L\pi)^{3/4} \exp\big(-2/L(x - q(t))^2 + ip_i(t)x\big), \qquad (1)$$

being propagated in time and space, undergoing collisions with nucleons in the nuclear medium in the process. Here x and t are space and time coordinates, and q_i and p_i describe the nucleon's position in configuration and momentum space.

The total wave function is assumed to be the direct product of the wave functions of the participating nucleons and hadrons. Participating means that they are either primary particles, or have been generated or scattered in the process of the cascade.

We do not take the Slater determinant into account in the description. The equations of motion factorize. For the above waveform, they have the same structure as the classical Hamilton equations, and can be solved using the well-known numerical integration methods of the cascade transport approach.

In Binary Cascade, unlike in QMD where the Hamiltonian can be looked at as self-generating from the system configuration, the Hamiltonian is calculated from simple, time-independent optical potentials. In addition, only participating hadrons are propagated, while nucleons in the nuclear model that are not participating in binary reactions are simply viewed as a representative nucleon configuration.

The imaginary part of the R-matrix acts like a scattering term. It is included in the model using discrete, binary reactions, *i.e.* 2-body scattering and particle decay. Free 2-body cross-sections are used and a geometrical interpretation of the cross-section is applied. Decay widths for strong resonances are effective decay widths at the resonances' stochastic masses.

For each of the above, a more detailed description will be given in the following sections.

The work was done in the context of the GHAD [3] frameworks of the GEANT4 [4] simulation toolkit. Software implementing the model is publicly available for an

[a] e-mail: Hans-Peter.Wellisch@cern.ch

independent verification of our results. It was released with GEANT4 in its 6.0 release.

2 Modeling overview

Binary Cascade is an intra-nuclear cascade propagating primary nucleons and all secondary particles within a nucleus. Interactions take place between a primary or secondary particle and an individual nucleon of the nucleus.

The nucleus is modeled by explicitly positioning nucleons in space, and assigning momenta to these nucleons. This is done in a way consistent with the nuclear density distributions, Pauli's exclusion principle, and the total nuclear mass. Details of the algorithm used are specified in later sections of this paper.

Free hadron-hadron elastic and reaction cross-section are used to define collision locations within the nuclear frame. Where available, experimental cross-sections are used directly or as a basis for parameterizations used in the model. Data were taken from the PDG [5] and CERN/HERA [6] collections.

Propagating particles in the nuclear field is done by numerically solving the equations of motion, using time-independent fields derived from optical potentials.

The cascade begins with a projectile and the nuclear description, and terminates when the average energy of all participants within the nuclear boundaries are below a given threshold. The remaining pre-fragment will be treated by pre-equilibrium decay and de-excitation models described elsewhere [7].

2.1 The transport algorithm

The initial condition of the transport algorithm is the primary particle's type and energy, and a 3-dimensional model of a nucleus.

For the primary particle an impact parameter is chosen randomly on a disk outside the nucleus, perpendicular to a vector passing through the center of the nucleus. The initial direction of the primary is perpendicular to this disk.

Using straight-line transport, the distance of closest approach $d_i^{\min}$ to each nucleon i in the target nucleus, and the corresponding time-of-flight t_i^d is calculated. The interaction cross-section σ_i with target nucleons is calculated based on the momenta of the nucleons in the nucleus, and the projectile momentum. Target nucleons for which the distance of closest approach $d_i^{\min}$ is smaller than $d_i^{\min} < \sqrt{\frac{\sigma_i}{\pi}}$ are candidate collision partners for the primary. All candidate collisions are ordered by increasing t_i^d. In case no collision is found, a new impact parameter is chosen. This way transparency effects at the nuclear boundaries are taken into account.

The primary particle is then transported in the nuclear field by the time step given by the time to closest approach for the earliest collision candidate. Outside the nucleus, particles travel along straight-line trajectories. Particles entering the nucleus have their energy corrected for Coulomb effects. Inside the nucleus particles are propagated in the nuclear field. The equation of motion in the field is solved for a given time step using a Runge-Kutta integration method.

At the end of each step, the interaction of the collision partners is simulated using the scattering term described below, resulting in a set of candidate particles for further transport. The secondaries from a binary collision are accepted subject to Pauli's exclusion principle. If the momentum of any of the particles is below the Fermi momentum, the interaction is suppressed, and the original primary continues to the time of its next collision. In case an interaction is Pauli allowed, the tracking of the primary ends, and the secondaries are treated like the primary. All their possible binary collisions with the residual nucleus are calculated, with the addition of decay in case of strong resonances. Note that, unlike in QMD, collisions between participants are not considered, limiting the applicability of the model to small participant densities.

For resonance decay, the collision time is the time to the decay of the particle, sampled from the resonance's lifetime. Herein the stochastic masses and decay widths are taken into account. All secondaries are tracked until they react, decay or leave the nucleus, or until the cascade stops due to the cut-off condition described above.

2.2 The description of the target nucleus and Fermi motion

A 3-dimensional model of the nucleus is constructed from A nucleons and Z protons with coordinates $\mathbf{r}_i$ and momenta $\mathbf{p}_i$, with $i = 1, 2, \ldots, A$.

Nucleon radii r_i are selected randomly in the nucleus rest frame according to the nuclear density $\rho(r_i)$. For nuclei with $A > 16$ we use a Woods-Saxon form of the nucleon density [8],

$$\rho(r_i) = \frac{\rho_0}{1 + \exp\left[(r_i - R)/a\right]}, \tag{2}$$

where ρ_0 is approximated as

$$\rho_0 = \frac{3}{4\pi R^3}\left(1 + \frac{a^2\pi^2}{R^2}\right)^{-1}. \tag{3}$$

Here $a = 0.545\,\mathrm{fm}$, and $R = r_0 A^{1/3}\,\mathrm{fm}$ with the correction $r_0 = 1.16(1 - 1.16A^{-2/3})\,\mathrm{fm}$.

For light nuclei we use a harmonic-oscillator shell model for the nuclear density [9],

$$\rho(r_i) = \left(\pi R^2\right)^{-3/2} \exp\left(-r_i^2/R^2\right), \tag{4}$$

where $R^2 = \frac{2}{3}\langle r^2\rangle = 0.8133 \cdot A^{2/3}\,\mathrm{fm}^2$. To take into account the repulsive core of the nucleon-nucleon potential we assume a minimum inter-nucleon distance of 0.8 fm.

The nucleus is assumed to be spherical and isotropic, *i.e.* we place each nucleon using a random direction and the previously determined radius r_i.

The momenta p_i of the nucleons are chosen randomly between 0 and the Fermi momentum $p_{\mathrm{F}}^{\max}(r_i)$. The Fermi momentum, in the local Thomas-Fermi approximation [10] as a function of the nuclear density ρ, is

$$p_{\mathrm{F}}^{\max}(r) = \hbar c\big(3\pi^2\rho(r)\big)^{1/3}. \tag{5}$$

The total vector sum of the nucleon momenta has to be zero, *i.e.* the nucleus must be constructed at rest. To achieve this, we choose one nucleon to compensate the vector sum of the remaining nucleon momenta $p_{\mathrm{rest}} = -\sum_{i=1}^{i=A-1} p_i$. If this sum is larger than the maximum allowable momentum $p_{\mathrm{F}}^{\max}(r)$, we iteratively flip the direction of the momenta of the nucleons with the largest contribution to the net nucleus momentum, until the residual sum is an allowed momentum value for a nucleon.

Special cases are introduced for ^{1}H, where the proton has momentum $p = 0$, and for the deuteron, where the momenta of proton and neutron are equal and in opposite direction.

2.3 Optical and phenomenological potentials

The effect of collective nuclear interaction upon participants is approximated by a time-invariant scalar optical potential, based on the properties of the target nucleus.

For protons and neutrons the potential used is determined by the local Fermi momentum $p_{\mathrm{F}}(r)$ as

$$V(r) = \frac{p_{\mathrm{F}}^2(r)}{2m}\,, \tag{6}$$

where m is the mass of the neutron or the mass of the proton, respectively.

For pions the potential used is a simple approximation given by the lowest-order optical potential as derived in [11]:

$$V(r) = \frac{-2\pi(\hbar c)^2 A}{\overline{m}_\pi}\left(1+\frac{m_\pi}{M}\right) b_0\rho(r). \tag{7}$$

Here A is the nuclear mass number, and m_π and M are the pion and nucleon masses, respectively. $\overline{m}_\pi$ is the reduced pion mass, $\overline{m}_\pi = (m_\pi m_N)/(m_\pi + m_N)$, where m_N is the mass of the nucleus. $\rho(r)$ is the nucleon density distribution. The parameter b_0 is the effective s-wave scattering length. The value used was obtained from the analysis to pion atomic data and resulted in b_0 to be about -0.042 fm.

2.4 Pauli-blocking simulation

The cross-sections and decay width provided by the scattering term used in this model are cross-sections of free particles. In the nuclear medium, these cross-sections are modified to effective cross-sections due to Pauli's exclusion principle.

For nucleons created in the process of the cascade, we check that all final-state nucleons occupy a state allowed by Fermi statistics. We assume that the nucleus is in its ground state and all states below Fermi energy are occupied. Thus we suppress collisions and decays for which any secondary nucleon has a momentum p_i below the local Fermi momentum, *i.e.*

$$p_i < p_{\mathrm{F}}^{\max}(r). \tag{8}$$

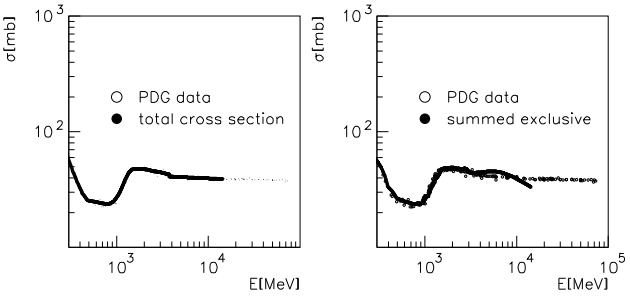

Fig. 1. Comparison of the total cross-section in pp scattering with experimental data from the Particle Data Group [5]. The dark lines represent the model information, and the small open circles represent the PDG data. The left plot shows the comparison with the total model cross-section, and the right plot shows the comparison with the sum of all exclusive-channel cross-sections considered in the final-state generation.

2.5 The collision condition

The basis of the description of the reactive part of the scattering amplitude are two-particle binary collisions, also with associated or direct resonance production, and decay. Based on the cross-section described later, collisions will occur when the transverse distance d_{t} of any participant target pair becomes smaller than the black-disk radius corresponding to the total cross-section σ_{t}

$$\frac{\sigma_{\mathrm{t}}}{\pi} > d_{\mathrm{t}}^2\,.$$

2.6 Total inclusive cross-sections

Experimental data and parameterizations thereof are used in the calculation of the total, inelastic and elastic cross-section wherever available.

2.6.1 Hadron-nucleon scattering

For the case of proton-proton (pp) and proton-neutron (pn) collisions, as well as π^+- and π^--nucleon collisions, experimental data and parameterizations are readily available as collected by the Particle Data Group (PDG) [5] for both elastic and inelastic collisions. We use a tabulation based on a sub-set of these data for $\sqrt{s}$ below 3 GeV, and the PDG parameterization at higher energies.

Figure 1 shows a comparison of the Binary Cascade's total scattering cross-sections with data from the PDG.

We also show the corresponding sum of all exclusive channels' cross-sections. The comparison of the latter is remarkable, given the large number of exclusive channels contributing. It also defines an upper limit of applicability of the model. Below 10 GeV kinetic energy, the resonance contributions considered are wholly sufficient to describe the total cross-section.

2.7 Channel cross-sections

Most of the cross-sections of individual channels involving meson-nucleon scattering can be modeled as resonance excitation in the s-channel. This kind of interactions exhibits a resonance structure in the energy dependence of the cross-section, and can be modeled using the Breit-Wigner function

$$\sigma_{\mathrm{res}}(\sqrt{s}) = \sum_{FS} \frac{2J+1}{(2S_1+1)(2S_2+1)} \times \frac{\pi}{k^2} \frac{\Gamma_{IS}\Gamma_{FS}}{(\sqrt{s}-M_R)^2+\Gamma^2/4}\,. \tag{9}$$

Here $S1$ and $S2$ are the spins of the two fusing particles, J is the spin of the resonance, $\sqrt{s}$ the energy in the center-of-mass system, k the momentum of the fusing particles in the center-of-mass system, and Γ_{IS} and Γ_{FS} are the partial width of the resonance for the initial and final state, respectively. M_R is the nominal mass of the resonance.

The initial states included in the model at present include all pion-nucleon scattering channels. The product resonances taken into account are the Delta-resonances with masses 1232, 1600, 1620, 1700, 1900, 1905, 1910, 1920, 1930, and 1950 MeV, and the excited nucleons with masses of 1440, 1520, 1535, 1650, 1675, 1680, 1700, 1710, 1720, 1900, 1990, 2090, 2190, 2220, and 2250 MeV.

2.8 Mass-dependent resonance widths and partial widths

During the cascading, the resonances produced are assigned real, stochastic masses, with values distributed according to the production cross-section described above. The stochastic masses of these resonances may be small or large compared to the nominal value, and this implies for example that some channels may not be open for decay, and hence has to be corrected for. In more general terms it means, that the partial and total decay widths of a strong resonance will depend on the stochastic mass of the resonance. We are using the approach introduced in UrQMD [12] for calculating these widths,

$$\Gamma_{R\to 12}(M) = (1+r)\frac{\Gamma_{R\to 12}(M_R)}{p(M_R)^{(2l+1)}}\frac{M_R}{M} \times \frac{p(M)^{(2l+1)}}{1+r(p(M)/p(M_R))^{2l}}\,. \tag{10}$$

Table 1. Values of the parameters of the cross-section formula (11) for the individual reaction channels.

Reaction	α	β	γ
$\mathrm{pp}\to \mathrm{p}\Delta_{1232}$	25 mbarn	0.4 GeV	3
$\mathrm{pp}\to \Delta_{1232}\Delta_{1232}$	1.5 mbarn	1 GeV	1
$\mathrm{pp}\to \mathrm{pp}^*$	0.55 mbarn	1 GeV	1
$\mathrm{pp}\to \mathrm{p}\Delta^*$	0.4 mbarn	1 GeV	1
$\mathrm{pp}\to \Delta_{1232}\Delta^*$	0.35 mbarn	1 GeV	1
$\mathrm{pp}\to \Delta_{1232}\mathrm{N}^*$	0.55 mbarn	1 GeV	1

Here M_R is the nominal mass of the resonance, M the stochastic mass, p is the momentum in the center-of-mass system of the particles, l the angular momentum of the final state, and $r = 0.2$.

2.9 Resonance production cross-section in the t-channel

In the resonance production in the t-channel, single and double resonance excitations in nucleon-nucleon collisions are taken into account. The resonance production cross-sections are as much as possible based on parameterizations of experimental data [6] for proton-proton scattering. The formula used for parameterizing the cross-sections is motivated from the form of the exclusive production cross-section of the Δ_{1232} in proton-proton collisions:

$$\sigma_{AB} = 2\alpha_{AB}\beta_{AB}\frac{\sqrt{s}-\sqrt{s_0}}{(\sqrt{s}-\sqrt{s_0})^2+\beta_{AB}^2} \times \left(\frac{\sqrt{s0}+\beta_{AB}}{\sqrt{s}}\right)^{\gamma_{AB}}\,. \tag{11}$$

The parameters of the description for the various channels are given in table 1. For all other channels, the parameterizations were derived from these by adjusting the threshold behavior accordingly.

Cross-sections for the reminder of the channels are derived from those described above, by applying detailed balance. Iso-spin invariance is assumed. The formalism used to apply detailed balance is

$$\sigma(cd\to ab) = \sum_{J,M}\frac{\langle j_c m_c j_d m_d \parallel JM\rangle^2}{\langle j_a m_a j_b m_b \parallel JM\rangle^2} \times \frac{(2S_a+1)(2S_b+1)}{(2S_c+1)(2S_d+1)} \times \frac{\langle p_{ab}^2\rangle}{\langle p_{cd}^2\rangle}\sigma(ab\to cd). \tag{12}$$

Figure 2 illustrates the quality of the channel cross-sections by showing a comparison between the model and data for the case of Δ production. The points are the $\Delta++$ production cross-sections, scaled with the appropriate Clebsh-Gordon coefficient. The line is the Binary Cascade prediction of this cross-section, summed over all contributing exclusive channels. We find good agreement.

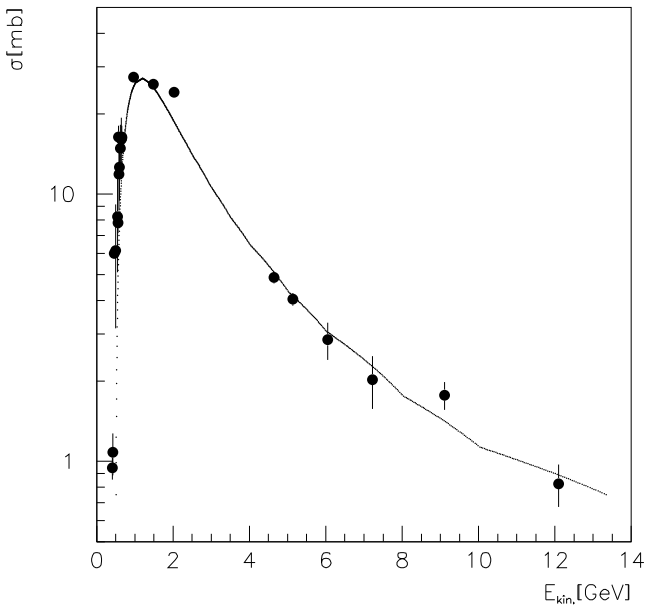

Fig. 2. Comparison of delta production cross-sections in pp scattering with experimental data from the CERN-HERA collections [6]. The points are the Δ++ production cross-sections, scaled with the appropriate Clebsh-Gordon coefficient. The line is the Binary Cascade prediction of this cross-section, summed over all contributing exclusive channels.

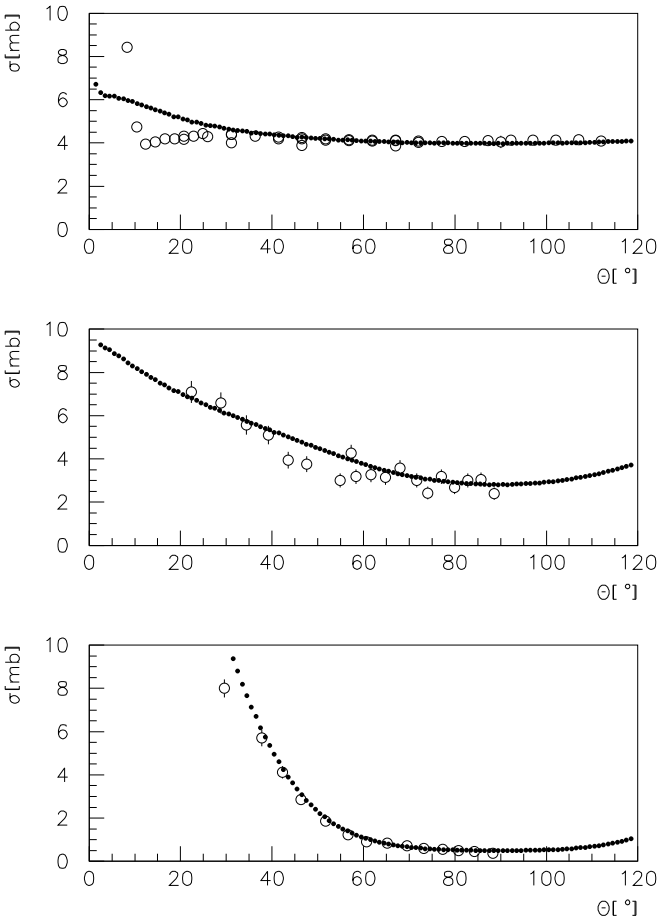

Fig. 3. Comparison of differential cross-section in pp elastic scattering with experimental data from the SAID data base [13]. The top plot shows the cross-section at 147 MeV energy, the middle plot shows the cross-sections at 597 MeV, and the lower plot shows the cross-sections at 1340 MeV. Open circles are data, full points are results of the model.

2.10 Nucleon-nucleon elastic final states

Angular distributions for elastic scattering of nucleons are taken as closely as possible from experimental data, *i.e.* from the result of a phase shift analysis. They are derived from differential cross-sections obtained from the SAID database, R. Arndt *et al.* [13].

Final states are obtained by sampling from tables of the cumulative distribution function (CDF) of the center-of-mass scattering angle, tabulated for a discrete set of lab kinetic energies. The CDFs are tabulated at 1 degree intervals and sampling is done using bi-linear interpolation in energy and CDF values. Coulomb and Coulomb interference effects are in this way taken into consideration automatically for the case of proton-proton scattering. Figure 3 compares the algorithm with experimental data from the SAID database.

2.11 Generation of transverse momentum

Angular distributions for final states other than nucleon-nucleon elastic scattering are calculated analytically, derived from the collision term of the in-medium relativistic Boltzmann-Uehling-Uhlenbeck equation [14] via scaling of the center-of-mass energy. This is done in analogy to UrQMD, based on the nucleon-nucleon elastic scattering cross-sections:

$$\sigma_{\mathrm{NN}\to\mathrm{NN}}(s,t) = \frac{1}{(2\pi)^2 s}(D(s,t) + E(s,t) + (\text{inverted } t,u)). \tag{13}$$

Here s, t, u are the Mandelstam variables, $D(s,t)$ is the direct term, and $E(s,t)$ is the exchange term, with

$$\begin{aligned} D(s,t) = {} & \frac{(g^{\sigma}_{\mathrm{NN}})^4(t-4m^2)^2}{2(t-m_\sigma^2)^2} \\ & + \frac{(g^{\omega}_{\mathrm{NN}})^4(2s^2+2st+t^2-8m^2s+8m^4)}{(t-m_\omega^2)^2} \\ & + \frac{24(g^{\pi}_{\mathrm{NN}})^4 m^4 t^2}{(t-m_\pi^2)^2} \\ & - \frac{4(g^{\sigma}_{\mathrm{NN}} g^{\omega}_{\mathrm{NN}})^2(2s+t-4m^2)m^2}{(t-m_\sigma^2)(t-m_\omega^2)}\,, \end{aligned} \tag{14}$$

and

$$
\begin{aligned}
E(s,t) = & \frac{(g^{\sigma}_{\mathrm{NN}})^4(t(t+s)+4m^2(s-t))}{8(t-m_\sigma^2)(u-m_\sigma^2)} \\
& + \frac{(g^{\omega}_{\mathrm{NN}})^4(s-2m^2)(s-6m^2)}{2(t-m_\omega^2)(u-m_\omega^2)} \\
& - \frac{6(g^{\pi}_{\mathrm{NN}})^4(4m^2-s-t)m^4t}{(t-m_\pi^2)(u-m_\pi^2)} \\
& + \frac{3(g^{\sigma}_{\mathrm{NN}}g^{\pi}_{\mathrm{NN}})^2m^2(4m^2-s-t)(4m^2-t)}{(t-m_\sigma^2)(u-m_\pi^2)} \\
& + \frac{3(g^{\sigma}_{\mathrm{NN}}g^{\pi}_{\mathrm{NN}})^2t(t+s)m^2}{2(t-m_\pi^2)(u-m_\sigma^2)} \\
& + \frac{(g^{\sigma}_{\mathrm{NN}}g^{\omega}_{\mathrm{NN}})^2(t^2-4m^2s-10m^2t+24m^4)}{4(t-m_\sigma^2)(u-m_\omega^2)} \\
& + \frac{(g^{\sigma}_{\mathrm{NN}}g^{\omega}_{\mathrm{NN}})^2((t+s)^2-2m^2s+2m^2t)}{4(t-m_\omega^2)(u-m_\sigma^2)} \\
& + \frac{3(g^{\omega}_{\mathrm{NN}}g^{\pi}_{\mathrm{NN}})^2m^2(t+s-4m^2)(t+s-2m^2)}{(t-m_\omega^2)(u-m_\pi^2)} \\
& + \frac{3(g^{\omega}_{\mathrm{NN}}g^{\pi}_{\mathrm{NN}})^2m^2(t^2-2m^2t)}{(t-m_\pi^2)(u-m_\omega^2)} \,.
\end{aligned}
\tag{15}
$$

In praxi, the in-medium mass, m, was set to the free nucleon mass value, and the nucleon-nucleon coupling constants used were 1.434 for the π, 7.54 for the ω, and 6.9 for the σ.

Finite-size effects were included at the meson-nucleon vertex, using a phenomenological form factor.

2.12 Resonance decay

In the decay of strong resonances, we use the decay branching ratios from PDG. All decay channels with nominal branching ratios larger than 1% are simulated.

The stochastic mass of an individual resonance created is sampled on creation from the Breit-Wigner form, under the mass constraints posed by the center-of-mass energy of the scattering, and the mass in the lightest-decay channel. The decay widths and partial widths are then adjusted according to eq. (10) to take the stochastic mass value into account.

2.13 The escaping particle and coherent effects

When a particle crosses the nuclear boundary, the ground state of the residual changes. This is a coherent effect that needs to be taken into account to describe the high-energy limit of particle production correctly. The energy of the outgoing particle could otherwise be such that the total energy available for the residual nucleus is below its ground-state mass. We hence adjust the energy of particles crossing the nuclear boundaries by the mass difference of old and new nucleus.

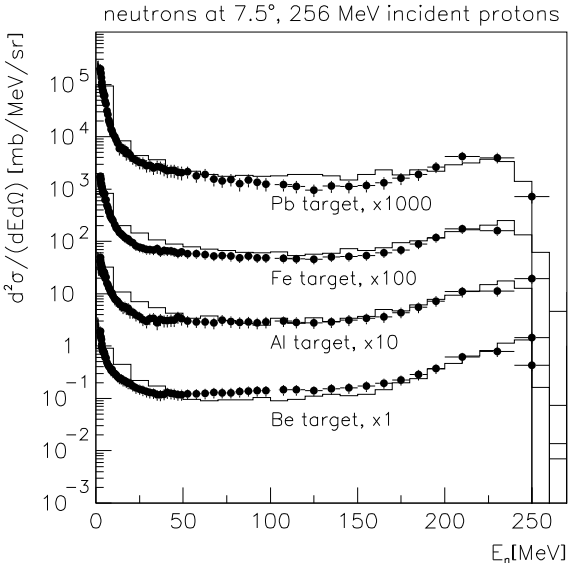

Fig. 4. Double differential cross-section for neutrons produced in proton scattering at 7.5 degrees by 256 MeV protons. Histograms: Binary Cascade predictions, points: data [15].

2.14 Transition to pre-compound modeling

Eventually, the cascade assumptions will break down at low energies, and the state of affairs has to be treated by other means such as evaporation and pre-equilibrium decay. This transition is not studied in depth at present, and interesting approaches of using the tracking time, as done in the Liege cascade code [16], can be applied.

For the purpose of this work, a simple algorithm suffices to determine when cascading is stopped: As long as the kinetic energy of the participants is above a certain threshold (70 MeV), the cascading continues.

The residual participants and the nucleus in its current state are then used to define the initial state for pre-equilibrium decay.

2.15 Calculation of excitation energies and residuals

At the end of the cascade, we form a pre-fragment for further treatment in pre-compound and nuclear de-excitation models.

These models need information about the nuclear fragment created by the cascade. The fragment is characterized by the number of nucleons in the fragment, the charge of the fragment, the number of holes, the number of all excitons, the number of charged excitons, and the four-momentum of the fragment.

The number of holes is given by the difference of the number of nucleons in the original nucleus and the number of residual nucleons in the pre-fragment. Nucleons captured in the pre-fragment at the end of the cascade are considered as excitons.

The momentum of the fragment, calculated by the difference between the momentum of the primary and the

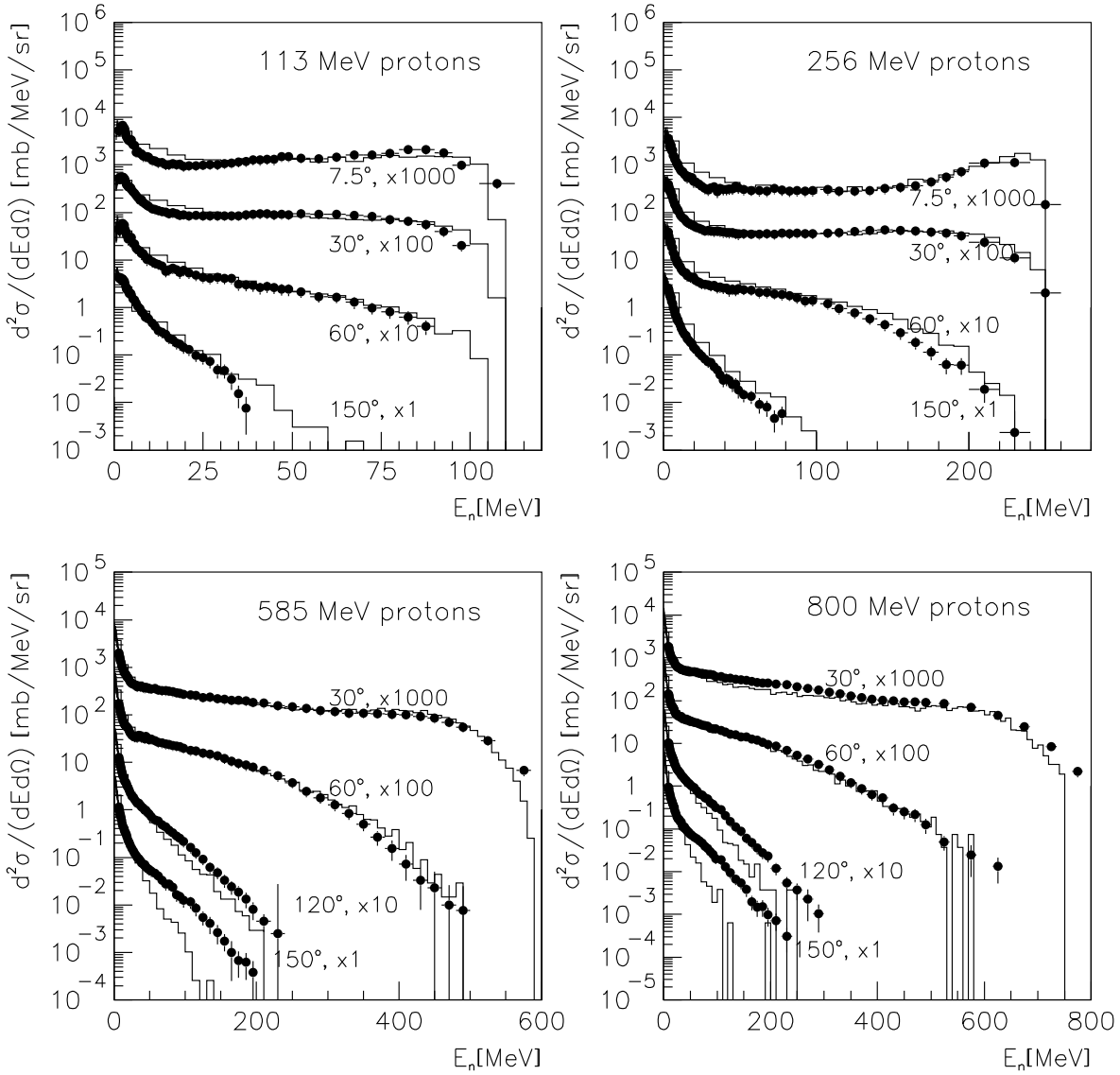

Fig. 5. Double differential cross-section for neutrons produced in proton scattering off aluminum. Histograms: Binary Cascade predictions, points: data [17,15,18,19].

outgoing secondary particles, is split into two components. The first is the momentum acquired by coherent elastic effects, and the second is the momentum of the excitons in the nucleus' rest frame. Only the latter part is passed to the de-excitation models.

3 Comparison with experiment

A verification suite [20] has been developed to evaluate and optimize hadronic models in the cascade energy range in GEANT4. The verification is done by comparing simulation results with experimental data from thin target measurements, mainly as collected in the EXFOR database [21]. At the time of writing, only data from measurements of absolute differential cross sections are utilized in the suite.

The modular structure of GEANT4 allows the generation of single events with a known incident particle energy and any explicitly defined hadronic final-state generator. The kinematics of secondaries produced in the interaction are then analyzed and the resulting angular, momentum, energy, and baryon number spectra are stored in histograms. The energy-momentum balance can be controlled as well. The histograms are compared to published measurements of the differential and double differential cross-sections, $\mathrm{d}\sigma/\mathrm{d}E$, $\mathrm{d}\sigma/\mathrm{d}\Omega$, $\mathrm{d}^2\sigma/\mathrm{d}E\,\mathrm{d}\Omega$, and the invariant cross-sections, $E\,\mathrm{d}^3\sigma/\mathrm{d}^3p$.

Some results produced with the Binary Cascade for the GEANT4 release 6.0 are presented in the following, focusing on neutron and pion production.

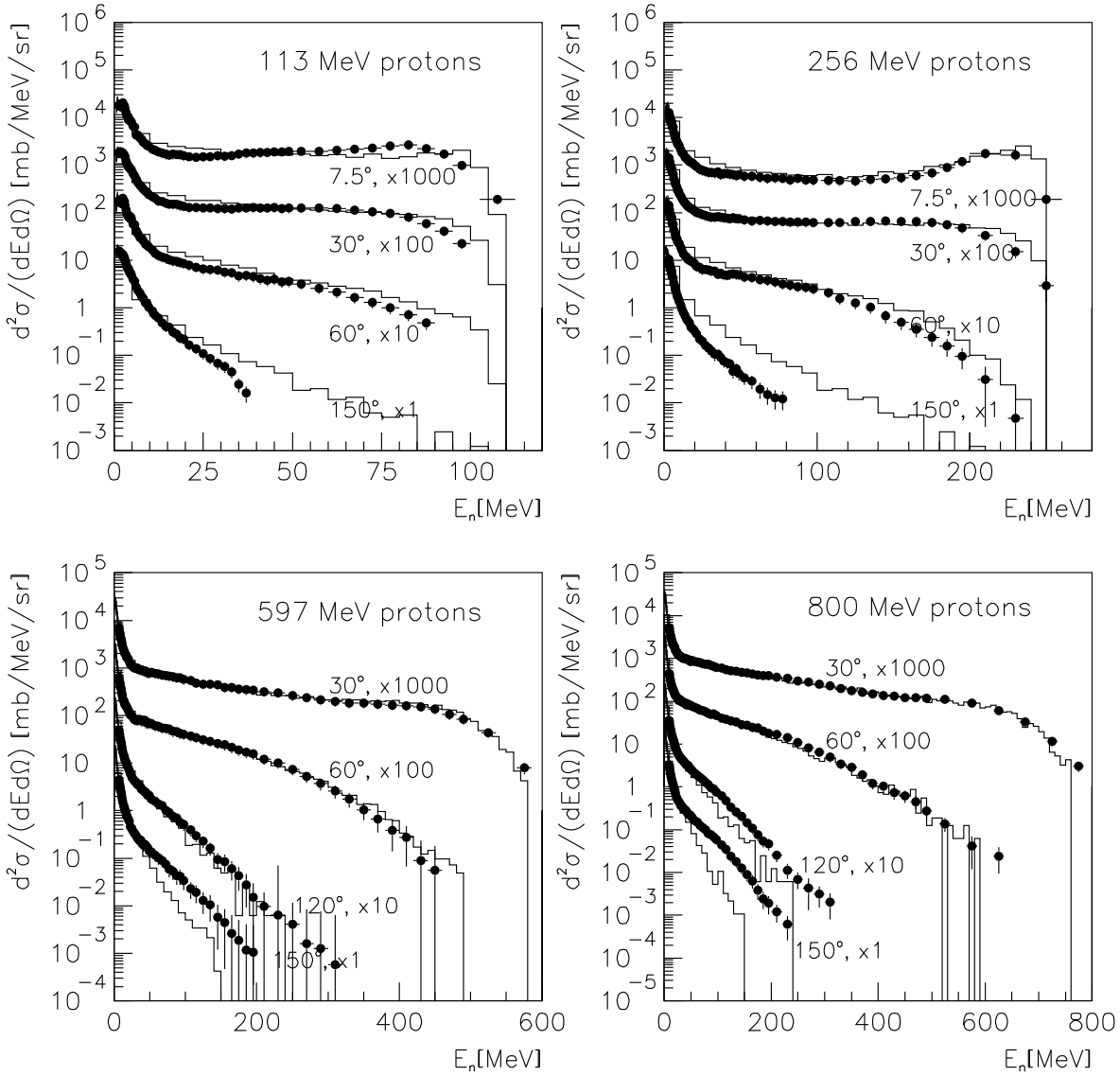

Fig. 6. Double differential cross-section for neutrons produced in proton scattering off iron. Histograms: Binary Cascade predictions, points: data [17,15,18,19].

Table 2. Cases contained in the verification for neutron production by incident protons on various target nuclei.

Nucleus	Beam energy (MeV)
Be	113, 256, 585, 800
C	113, 256, 590
Al	22, 39, 90, 113, 160, 256, 585, 800
Fe	22, 65, 113, 256, 597, 800
Ni	585
Zr	22, 35, 50, 90, 120, 160, 256, 800
Pb	35, 65, 113, 120, 160, 256, 597, 800

3.1 Neutron production

Verifications have been performed for neutrons produced by protons incident upon various targets for proton energies below 1 GeV. In this energy region the inclusive reaction channel

$$\mathrm{p} + A \longrightarrow \mathrm{n} + X, \tag{16}$$

has been studied experimentally for many years, and a rich body of experimental data is available. The secondary neutrons can be identified and their energies can be measured with good precision using time-of-light techniques. A significant number of test cases have been created (table 2). We show comparisons for a few representative situations.

In particular the high-energy part of the double differential inclusive neutron spectra is very sensitive to the physics model used in the cascade code.

Figure 4 shows double differential cross-sections for proton-induced neutron production at forward angles for several materials. We are using linear scale to put

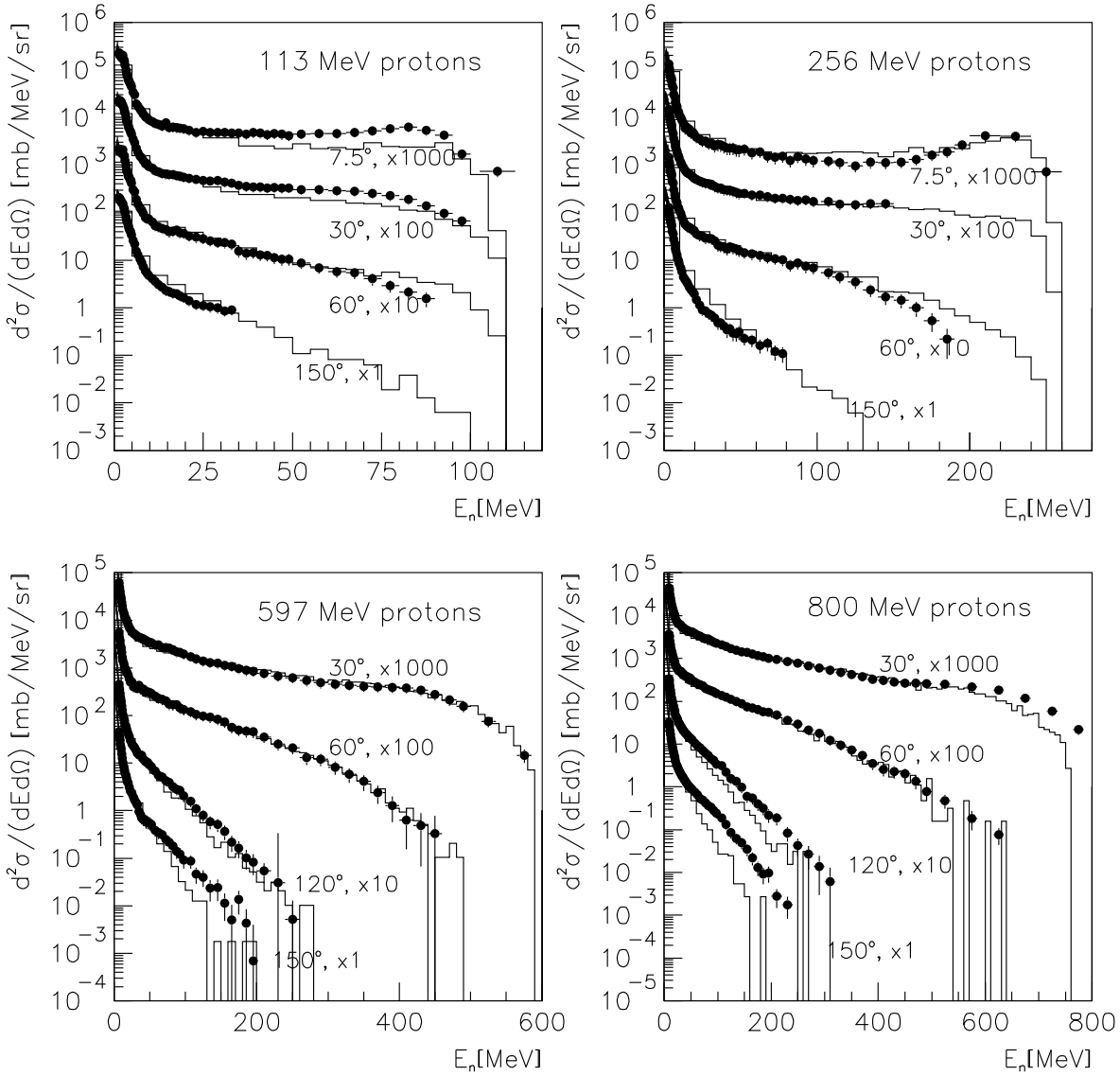

Fig. 7. Double differential cross-section for neutrons produced in proton scattering off lead. Histograms: Binary Cascade predictions, points: data [17,15,18,19].

emphasis onto the cascade energy regime, where mostly the proton creates an energetic neutron at small angles in a charge exchange reaction. The figure shows that the quality of the description of the forward peak is very good for a wide range of materials. Also the plateau at intermediate energies is well described.

Figures 5, 6, and 7 show comparisons of neutron double differential cross-sections at several angles, and for several incident proton energies in three materials, Al, Fe, and Pb, respectively.

We find an excellent agreement between data and model for all energies and materials, with the exception of high-energy neutrons at large neutron scattering angles in heavy materials. Given the conceptual absence of S-wave pion re-absorption on quasi-deuterons in the model, the agreement is expected to be reduced in quality at large angles for incident proton energies above the pion production threshold, in particular for large nuclei. There we expect the model prediction to be lower than the experimental data.

3.2 Pion production

In the before-mentioned GEANT4 verification suite, a sizable set of comparisons of pion productions is available (table 3) for the reactions

$$\mathrm{p} + A \longrightarrow \pi^{\pm} + X. \tag{17}$$

Due to the before mentioned conceptual absence of S-wave pion re-absorption on quasi-deuterons in the

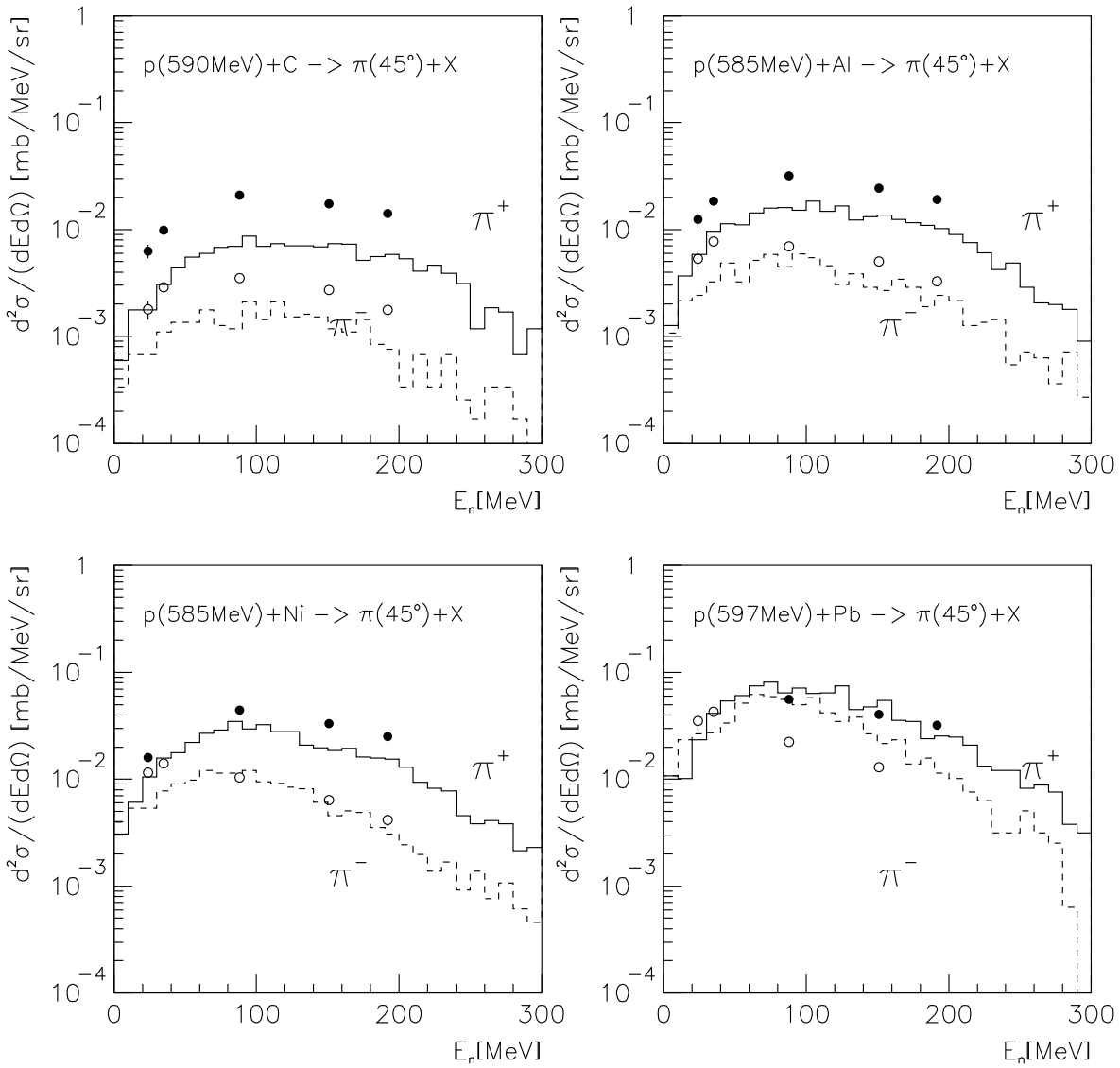

Fig. 8. Double differential cross-section for pions produced at 45° in 597 MeV proton scattering off various materials. Histograms: Binary Cascade predictions, points: data [22].

Table 3. Cases contained in the verification for pion production by incident protons on various target nuclei.

Target nucleus	Beam energy (MeV)
H	585
D	585
Be	585
C	590
Al	585, 730, 1000
Cu	730
Ni	200, 585
Pb	585, 730

model, we give just one comparison in fig. 8. It shows the double differential cross-sections for the production of π^+ and π^- on various materials at 585 MeV proton incident energy for a selected angle. Data were taken from [22].

The overall agreement between prediction and experiment is found to be reasonable. The experimental cross-sections show that π^+ production by protons is significantly larger than π^- production. This feature is well-reproduced by Binary Cascade. The dependence of the cross-section on the pion energy is also well reproduced, although the overall normalization is underestimated for positive pions by a factor of about 1.5–3 for carbon and aluminum. It is interesting to see how for heavier elements an excess of low-energy pions is showing in the model result. The effect is stronger for negative pions than for positive pions, and we tend to associate it to the absence of the re-absorption channel mentioned above.

4 Conclusions

The Binary Cascade intra-nuclear transport model was described. It mixes the approaches of QMD and generalized cascades, and comes with a large, resonance-based collision term. The range of its applicability in nucleon nuclear reactions stretches from $< 100\,\mathrm{MeV}$ to about $10\,\mathrm{GeV}$, allowing for a consistent calculation of the secondary hadron spectra in the low and intermediate energy domains. Extensions of this term to cover pion-induced reactions and strangeness are in discussion.

Comparisons to experimental data for neutron and pion production in proton nuclear reactions have been presented. The predictive power of the approach is quite convincing, in particular in the high-energy part of the spectra, where cascade codes otherwise often experience limitations in the quality of description.

The Binary Cascade model implementation in GEANT4 has no fixed structure. It was designed to serve as a proving ground of new concepts and theoretical ideas in the intermediate-energy domain.

The authors wish to thank Dr D.H. Wright and Dr T. Koi of SLAC for their contributions to the GEANT4 verification suite for the cascade energy range, and Dr Henning Weber of Frankfurt University for many useful discussions concerning UrQMD. The assistance of Prof. G. Greeniaus of the University of Alberta and TRIUMF in accessing and using the SAID database was invaluable.

References

1. S.G. Mashnik, A.J. Sierk, J. Nucl. Sci. Tech. **S2**, 720 (2002); T.A. Gabriel, ORNL/TM-9727, *Proceedings of LEP Experimenters' Workshop on Shower Simulation, Geneva, Switzerland, January 29-31, 1985*; J. Cugnon, C. Volant, S. Vuillier, Nucl. Phys. A **620**, 475 (1997); Y. Nara, N. Otuka, A. Ohnishi, K. Niita, S. Chiba, Phys. Rev. C **61**, 024901 (2000); G. Peter, D. Behrens, C.C. Noack, Phys. Rev. C **49**, 3253 (1994); Hai-Qiao Wang, Xu Cai, Yong Liu, High Energy Phys. Nucl. Phys. **16**, 101 (1992); A.S. Ilinov, A.B. Botvina, E.S. Golubeva, I.A. Pshenichnov, Sov. J. Nucl. Phys. **55**, 734 (1992); A.V. Dementev, N.M. Sobolevsky, Nucl. Tracks Radiat. Meas. **30**, 553 (1999); A. Fasso *et al.*, SLAC-REPRINT-1997-090 prepared for *the 3rd Workshop on Simulating Accelerator Radiation Environments (SARE3), Tsukuba, Japan, 7-9 May 1997*; D.V. Gorbatkov, V.P. Kryuchkov, Nucl. Instrum. Meth. A **374**, 95 (1996); J.F. Briesmeister, LA-7396-M, Rev. 2 and citations therein.
2. M. Bleicher *et al.*, J. Phys. G **25**, 1859 (1999); H. Sorge, Phys. Rev. C **52**, 3291 (1995); K. Niita *et al.*, Phys. Rev. C **52**, 2620 (1995); C. Hartnack, PhD Thesis, University of Frankfurt (1993); GSI Report 93-05; Jörg Aichelin, Phys. Rep. **202**, 233 (1991).
3. J.P. Wellisch, Comput. Phys. Commun. **140**, 65 (2001).
4. GEANT4 Collaboration (S. Agostinelli *et al.*), Nucl. Instrum. Meth. A **506**, 250 (2003).
5. Particle Data Group Collaboration (K. Hagiwara *et al.*), Phys. Rev. D **66**, 1 (2002).
6. CERN High Energy Analysis Group records, preprint denominations CERN-HERA-YY. For example, E. Bracci, C. Burichetti, J.P. Droulez, E. Flaminio, C. Preti, *Compilation of Differential Cross-Sections. Pi Induced Reactions.*
7. V. Lara, J.P. Wellisch, published in *Annecy 2000, Proceedings of the IX International Conference on Calorimetry in High Energy Physics, Annecy, France, 9-14 October, 2000*, Frascati Phys. Ser., Vol. **XXI** (2001) p. 449.
8. M.E. Grypeos, G.A. Lalazissis, S.E. Massen, C.P. Panos, J. Phys. G **17**, 1093 (1991).
9. L.R.B. Elton, *Nuclear Sizes* (Oxford University Press, Oxford, 1961).
10. A. DeShalit, H. Feshbach, *Theoretical Nuclear Physics*, Vol. **1**: *Nuclear Structure* (Wyley, 1974).
11. K. Stricker, H. McManus, J.A. Carr, *Nuclear scattering of low energy pions*, Phys. Rev. C **19**, 929 (1979).
12. M. Bleicher *et al.*, J. Phys. G **25**, 1859 (1999).
13. R.A. Arndt, I.I. Strakovsky, R.L. Workman, Int. J. Mod. Phys. A **18**, 449 (2003).
14. G.F. Bertsch, S. Das Gupta, Phys. Rep. **160**, 189 (1988); W. Cassing, U. Mosel, Prog. Part. Nucl. Phys. **25**, 235 (1990); T. Maruyama, W. Cassing, U. Mosel, S. Teis, Prog. Theor. Phys. Suppl. **120**, 283 (1995).
15. M.M. Meier *et al.*, *Differential neutron production cross sections for 256-MeV protons*, Nucl. Sci. Eng. **110**, 289 (1992).
16. J. Cugnon, C. Volant, S. Vuillier, Nucl. Phys. A **620**, 475 (1997).
17. M.M. Meier *et al.*, *Differential neutron production cross sections and neutron yields from stopping-length targets for 113-MeV protons*, Nucl. Sci. Eng. **102**, 310 (1989).
18. W.B. Amian *et al.*, *Differential neutron production cross sections for 597-MeV protons*, Nucl. Sci. Eng. **115**, 1 (1993).
19. W.B. Amian *et al.*, *Differential neutron production cross sections for 800-MeV protons*, Nucl. Sci. Eng. **112**, 78 (1992).
20. V. Ivanchenko *et al.*, *The GEANT4 hadronic verification suite for the cascade energy region.* Talk given at the Conference for Computing in High-Energy and Nuclear Physics (CHEP03), La Jolla, CA, USA, 24-28 March 2003. e-Print Archive: physics/0306016.
21. EXFOR database. `http://www.nea.fr/html/dbdata/x4/welcome.html`
22. J.F. Crawford *et al.*, *Measurement of cross sections and asymmetry parameters for the production of charged pions from various nuclei by 585-MeV protons*, Phys. Rev. C **22**, 1184 (1980).